Systematic variations in polymer gel dosimeter calibration due to container influence and deviations from water equivalence.

ML Taylor[1*], RD Franich[1], PN Johnston[1], RM Millar[2] and JV Trapp[1]

[1]*Applied Physics, RMIT University, GPO Box 2476V, Melbourne, Victoria 3001, Australia*
[2]*William Buckland Radiotherapy Centre (WBRC), The Alfred Hospital, PO Box 315, Prahran, Victoria 3181, Australia*

Abstract

There are a number of gel dosimeter calibration methods in contemporary usage. The present study is a detailed Monte Carlo investigation into the accuracy of several calibration techniques. Results show that for most arrangements the dose to gel accurately reflects the dose to water, with the most accurate method involving the use of a large diameter flask of gel into which multiple small fields of varying dose are directed. The least accurate method was found to be that of a long test tube in a water phantom, coaxial with the beam. The large flask method is also the most straightforward and least likely to introduce errors during setup, though, to its detriment, the volume of gel required is much more than other methods.

[*] Corresponding Author: Applied Physics, RMIT University, GPO Box 2476V, Melbourne 3001, Australia; Phone ++61 3 9925 2138; FAX ++61 3 9925 5290;
e-mail: michael.taylor@rmit.edu.au

1. Introduction

Gel dosimeters are often used for relative dosimetry; however for quantitative information it is necessary to calibrate each batch of gel individually. In principle, this is undertaken by irradiating gel with varying doses, with the assumption that the doses received are equivalent to that in water under the same conditions. A dose calibration curve is then constructed by association of the presumed dose at such points with the corresponding relaxation rate values obtained via MRI, or with Hounsfield units from x-ray computed tomography, attenuation coefficients from optical computed tomography, or similar. The importance of calibration is self evident and, in the case of gel dosimeters, uncertainty in calibration has been the subject of various studies (Baldock 1999, Trapp 2004a).

Fricke dosimeters and various polymer gels have been shown in previous studies to be effectively water equivalent (Keall and Baldock 1999) however, there has been comparatively little consideration of the effect of backscatter from containers on the absorbed dose in gel dosimeters. Michael *et al* (2000) concluded that the presence of glass containers and Nitrogen pockets therein had no significant effect on the *total* absorbed dose within a vial of gel. However, alternative calibration techniques and the local effects of containment vessels coupled with the compounded effects of juxtaposition of multiple containers have not been previously investigated in detail.

Numerous practical techniques for gel calibration exist. One method involves the use of multiple small vials in a water phantom that are given varying doses. This can be performed by irradiating each one individually, or by irradiation the entire batch of vials in dose increments and successively removing a vial from the batch between each increment. This is generally achieved by irradiating through the bases of the vials at a given depth within the water phantom, typically either at the surface (so that D_{max} is in the gel) or 5 cm below (region of near-linear dose gradient), where the doses in water are well known (Maryanski *et al* 1994). The result is a number of vials, each of which has received a different dose and thus yields a different calibration point (Baldock *et al* 1998 and 1999,).

A second dose calibration method employs a relatively large volume flask of gel placed in air, into which numerous small fields of varying doses are directed (Maryanski *et* al 1994, Oldham *et al* 1998a). D_{max} is typically the calibration point for this technique. A variation of this method uses fields incident on the sides of the flask such that they intersect centrally creating a spoke-like pattern (Maryanski *et al* 1996).

A further method uses long gel-filled test tubes placed within a water phantom and irradiated through the bases so that a depth-dose distribution exists along the length of the tube. The long dose distribution allows multiple calibration points to be obtained from a single test tube (Oldham *et al* 1998b).

Another method involves gel-filled test tubes placed 5 cm deep in a water phantom with their axes perpendicular to the irradiation field (McJury *et al* 1999a, Vergote *et al* 2004). This allows data along the test tube axis to be averaged in order to reduce uncertainties. Test tube diameters are typically of the order of 2.5 cm, though tubes of internal diameters as small as 10 mm have been employed (DeDeene *et al* 2001).

Trapp *et al* (2004b) used dose area histogram equalisation with films to calibrate MAGIC gel (Fong *et al* 2001), and methods using planned doses within a phantom have also been employed (Love *et al* 2003, Trapp *et al* 2004c). The advantage of these methods is that calibration is performed within the phantom itself, thus eliminating possible errors resulting from differences in post-manufacture temperature history between the phantom and the calibration gels (DeDeene *et al* 2000)

The fact that such a wide range of dose calibration techniques exists implies that an optimal method has not yet been identified. Monte Carlo simulation presents an ideal mechanism for investigation of such calibration methods, given that accurate experimental validation would be technically difficult. In this work we examine the accuracy of some of the calibration techniques via Monte Carlo modelling, employing the Electron Gamma Shower (EGSnrc) code developed by the Stanford Linear Accelerator Centre (SLAC) and the National Research Council of Canada (Nelson *et al*). It is well accepted that Monte Carlo generates accurate dose calculations, even in zones of electronic disequilibrium, such as interfaces between materials of high and low density. In this work, several of the aforementioned gel calibration arrangements are modelled to determine the extent to which containment vessels affect the absorbed dose in gel dosimeters. This allows an informed choice between the common dose calibration methods to minimise the systematic errors introduced by calibration.

2. Methods

2.1 Overview

The DOSRZnrc user code for EGSnrc was employed, allowing dose to be scored in detailed cylindrical geometries. Dose deposition was modelled in six of the arrangements that are representative of the primary techniques in practical usage, including ‘small vials’, ‘large flask’ and the two test tube arrangements described above. Statistical uncertainty in the dose relates to the fluence of radiation within a given region of a model. The cylindrical nature of the geometries means that regions along the axes of symmetry in the models presented here have proportionally lower fluence than the surrounding annuli, and thus typically have greater uncertainty. In depth dose curves along the axes of symmetry this uncertainty was 0.25 % or less at D_{max}. Simulation times varied between four and sixty hours using a 2.4 GHz AMD Opteron dual processor. In all cases an

equivalent exposure in 'water only' was simulated for comparative purposes. Note that although polymer gels undergo a density change after being subjected to radiation (Trapp *et al* 2001, Trapp *et al* 2002), for the purpose of this work it is assumed that such changes do not occur during the irradiation.

2.2 Composition of Materials

PEGS4 data sets are available with the standard EGSnrc release, containing compositional details and stopping powers for various materials. Where standard PEGS4 material data files were unavailable, these were generated from National Institute of Standards and Technology (NIST) data (NIST website). However, for electrons passing through a material with energies above one MeV, the electric fields of increasingly distant orbital electrons are felt as a result of relativistic effects, causing an increase in the mass collision stopping power (Metcalfe *et al* 1997). The extent of this effect is dependant upon the density of the medium; hence it is referred to as the 'density effect'. This was accounted for by corrections to the stopping power, calculated using NIST data, though at the energies used here the effect is not significant and such corrections are not essential. Polyacrylamide gel (PAG) is a widely used gel, including three of the six published methods studied in this work. PAG has been utilised in all models presented here to allow direct comparison between the different calibration methods. The models use the composition outlined by Maryanski *et al* (1993) with a density of 1.02 $kg.m^{-3}$, the details of which are given in Table 1.

2.3 Source

6 MV photon fields are commonly used in calibration of gel dosimeters. It is the authors' intention that this work be as readily reproducible as possible; the models thus employ the 6 MV photon spectrum by Mohan *et al* (1985) which is available online with the standard EGSnrc package (EGS website). Consistent with the cylindrical geometries modelled, the sources employed are circular beamspots of various diameters.

2.4 Vial geometries

The vial modelled is a Pyrex (borosilicate) glass vial of internal diameter 25 mm and length 55 mm, with a polyethylene cap. The thickness of the vial base and walls is 1 mm. The vial is submerged in a water phantom of lateral dimensions five times that of the vial, which is located centrally. A 10 cm diameter circular field is incident on the surface, irradiating the vial through its base. Results are presented for two cases: the first with the vial placed at the water surface such that D_{max} occurs within the gel ('Method A'); the second with the vial at a depth of 5 cm, such that the dose gradient within the gel is fairly linear ('Method B'). These two geometries are shown in Figures 1 (a) and (b) respectively.

2.5 Test tube geometries

The test tube modelled is a Pyrex culture tube with a polyethylene screw-top lid, 200 mm long with an internal diameter of 25 mm and a wall thickness of 1 mm, comparable to that used by Oldham *et al* (1998b) experimentally. The test tube is immersed in a water phantom in two geometries: the first with the test tube at the water surface centrally located in the water phantom and coaxial with the beam ('Method C'; see Figure 1(c)). The second case models the test tube 5 cm deep, with its axis perpendicular to that of the beam ('Method D'; see Figure 1(d)). This method simulates a parallel opposed pair of beams with the central axis of the dosimeter at the centre of the water tank (due to volume averaging of the axial voxels). A further model was run in the latter arrangement, with a test tube of internal diameter 10 mm and length 100 mm – similar to that used by DeDeene (2001) ('Method E'; see Figure 1(e)). The beam spot size radii employed were 50 mm in the coaxial case, 150 mm for the large perpendicular test tube and 100 mm for the small perpendicular test tube.

2.6 Large flask geometry

The large flask modelled here is based on specifications for a Perspex tub used experimentally by Oldham *et al* (1998a). The flask is cylindrical, with a circular base of inner diameter 130 mm and wall thickness 6 mm. The gel is 40 mm thick within the flask, after which there is a 5 mm nitrogen gap. The presence of nitrogen is a result of the necessity to fill the flask with gel in an oxygen-free environment. In the case of test tubes and vials, the vessels are typically over-filled with gel such that when the lid is screwed on there is negligible nitrogen present within the container. Models were run both with and without the nitrogen gap.The total height of the flask, including walls, is 57 mm. The flask is placed in air and irradiated through the base with a 2 cm radius field ('Method F'; see Figure 1(f)). While there are considerable uncertainties associated with delivering known doses to small fields, performing comparative simulations normalises for these effects and the results represent the discrepancy due to container and gel effects only.

3. Results and Analysis

3.1 Overview

For each configuration, photon depth doses and profiles are given with water-only curves for comparison. Difference plots for each highlight the discrepancies that are the subject of this work. Radial plots show the range of influence of inhomogeneities such as container walls and show that, within the container, the measured dose to gel will be a function of the extent of the voxels that are volume-averaged.

3.2 Vial method

Figures 2(a)(i) and 3(a)(i) show the depth dose curves for Methods A and B respectively.. Figures 2(a)(ii) and 3(a)(ii) are plots of the ratio of the curves to the equivalent local dose values in water.

Figure 2(b)(i) shows the dose radially outward from the central axis of the vial at D_{max}. Similarly, Figure 3(b)(i) shows the radial dose distribution at a depth corresponding to the mid-point of the vial. The equivalent curve in water alone is also shown, and Figures 2(b)(ii) and 3(b)(iii) show the ratio of the depth dose curve in the vial system to that in water alone.

Inspection of the near-surface region of the depth dose curves shown in Figure 2 (a)(i-ii) highlights significant disparity between the dose to gel in a small vial placed at the surface of the water phantom and the water phantom alone. If a calibration point is chosen carefully at a depth of 1.5 cm (or slightly more) within the gel, the dose matches that in water to well within 1 %. However, taking a point at a shallower depth can lead to a difference between 2 and 20 %.

If the vial of gel is placed at a depth of 5 cm, inspection of Figure 3 indicates that the dose is generally one to two percent lower within the gel compared to that in water (this may be attributed to the slightly higher density of PAG). The sudden drop in dose at a depth of 5 cm corresponds to the glass base of the vial; following this, there is a small build-up region within the PAG.

The small vial method of calibration yields one calibration point per vial. The most appropriate approach for both arrangements (with the vial at the surface or at a depth of 5 cm) is to take an area of 80 mm^2 about the central axis of the vial and average the voxel values. If the vial is at the surface, this should be done at D_{max}, yielding a value that is 0.7 (± 0.2) % lower than the dose in water. If the vial is at a depth of 5 cm, then similarly averaging a slice of voxels in the middle of the vial yields a value lower than the dose to water by 0.4 (± 0.2) %.

3.3 Test tube (axis aligned with beam) method

Figure 4 (a)(i) shows the depth dose curve for Method C, plotted with the corresponding depth dose curve through water only. Figure 4 (a)(ii) shows the ratio of the former curve to the latter. The dose is also plotted as it varies radially outward from the central axis in this cylindrical geometry. As this differs with depth, radial dose distributions are given for three depths along the test tube: 5, 10 and 15 cm.

From inspection of Figure 4 (a)(i) it is clear that D_{max} occurs at a slightly shallower depth within the test tube compared to water, and after D_{max} the dose to the gel is consistently lower than that to water. Figure 4 (a)(ii) helps quantify this effect, displaying the ratio of dose in the test tube of gel to dose in water, which clearly exhibits a degree of depth dependence. Figures 4 (b)(i, iii and v) show the dose deposition radially outward from the central axis at depths of 5, 10 and 15 cm respectively. The prominent drop in dose at a radial distance of 1.25 cm is due to the presence of the glass wall. The radial dose behaviour is increasingly non-uniform at greater depths within the test tube. Carefully

choosing an area of 80 mm^2 about the central axis (approximately half the radial distance from the axis to the test tube wall) at a series of points at various depths along the test tube yields multiple calibration points. With depth, however, there is increasing disparity with the dose to water. This difference is quantified in Table 2 for the aforementioned depths.

3.4 Test tube (axis perpendicular to beam) method

Both Methods C and D involve a test tube placed 5 cm deep within a water phantom, with its axis perpendicular to that of the field. The two arrangements differ in the size of the test tube and the diameter of the beam, which in both cases is sufficiently large to blanket the test tubes. Fig 5 (a)(i) shows the central axis dose profile for Method C, while Fig 5 (b)(i) corresponds to Method D. The ratio of the dose in these arrangements to the dose in water alone is shown in Figs 5 (a)(ii) and 5 (b)(ii).

The results in Figure 5 indicate that the presence of glass and its curvature have a small effect on the dose absorbed along the centre of the test tube. It is not practical to try and extract information about the dose deposition radially out from the central axis because the beam was incident from one side only (not parallel-opposed) and hence the simplified RZ geometry of the model would not readily yield useful information. What is more useful from a practical perspective is knowledge of the average dose delivered to a finite volume down the central axis of the test tube. Figure 5 (b)(ii) exhibits greater statistical noise as a result of the small voxels used to define the detailed geometry.

A single calibration point can be obtained by taking an area about the centre and averaging along the axis of the test tube, avoiding regions towards the ends of the test tube which are subject to more pronounced scattering effects.

If the measurement is taken in this fashion for the 10 mm diameter test tube, averaging over a lateral area of 13 mm^2, the difference between dose to gel and the corresponding dose in water is 0.4 (± 0.2) %. In the case of the 25 mm diameter test tube, taking an average of 13 mm^2 along a length of 160 mm yields a value of dose lower than that in water by 0.7 (± 0.1) %.

3.5 Large flask method

The large flask modelled here, Method F, is representative of that used by Oldham *et al* (1998a). For greater generality, the results shown in Figure 6 correspond to a model with no nitrogen gap (i.e. filled entirely with gel). A further model has been run which more precisely represents the description given in (Oldham *et al* 1998a) which shows that the nitrogen gap does not significantly alter the dose distribution in the rest of the flask, and certainly not in the vicinity of D_{max}. Figure 6 (a)(i) shows the depth dose curve for the 2 cm radius field down the centre of the flask. Figure 6 (a)(ii) is the ratio of

the dose to the flask and the dose to water. Figure 6 (b)(i) shows the dose distribution radially outward from the central axis at a depth corresponding to D_{max}, with the equivalent curve in water. Similarly, Figure 6 (b)(ii) shows the ratio of the former curve to the latter.

The dose in the build-up region of the gel is several percent higher than that of water, however the dose matches well in the region of D_{max}; between depths of approximately 1 and 2 cm the dose is within 1 % of that in water. This is further verified by observation of Figure 6 (b)(ii) which shows the dose deposition radially outward from the central axis at D_{max}. Within the beamspot of radius 2 cm, the dose remains within 1 % of that to water. Inspection of Figure 6 (a)(ii) shows that if data is used from depths between 2 and 5 cm, the dose is 1 to 2 % lower than that in water. Taking an 80 mm^2 area at D_{max}, with a voxel thickness of 2 mm, shows that the average dose is 0.2 (± 0.1) % lower than that to water.

4. Discussion

The Monte Carlo investigation undertaken here shows that the majority of calibration methods examined in this work, if performed in a precise fashion, provide an accurate representation of the dose to water – within the 1 % confidence limit usually specified. Table 3 summarises various details of the gel calibration methods tested, such as vessel dimensions and model geometry, along with the measurement method and the disparity between the dose to gel and dose to water.

The relevant limitations of each calibration method can be categorised into the following: (i) the degree of influence of the containers on the absorbed dose, (ii) the number of calibration points that can be obtained for a given quantity of gel used and (iii) the potential for set-up error (including the influence on absorbed dose from neighbouring containers). The latter problem is analogous to that faced in radiotherapy of a patient.

The dose to gel is typically lower on the central axis and becomes higher near the container wall due to scattering contributions. However, in Method C, the dose near the test tube wall is reduced by the longer path length through the curved glass end of the tube. This means that in most cases, the choice of volume averaged in the dose measurement process will influence the result obtained. Knowledge of the radial distribution can be used to influence the magnitude of the disparity.

For the majority of calibration techniques examined, the effect of the container on the dose to the gel is minimal, provided measurements are taken at specific points. It is evident that in this regard the large flask of gel is the most accurate, as long as the set-up is precise and the post-irradiation measurement is taken carefully at D_{max}. Using a thin test tube with its axis perpendicular to the beam, or a small vial coaxial with the beam, at a depth of 5 cm below the water phantom surface also results

in doses that match that to water within half a percent. Using a small vial at the surface of the water phantom provides slightly less accurate results, though still well within 1 % of the dose to water. Irradiating a long test tube along its axis to achieve multiple calibration points is the least accurate in this sense, with local dose deposition in the gel differing from that to water to varying degrees along the length of the test tube as indicated by Figure 4 and Table 2.

To achieve a useful calibration curve, a number of calibration points are necessary. It would thus be desirable to employ a calibration method that uses as little gel as possible, particularly given that many centres do not have the capacity to produce large volumes of gel. Table 3 shows the approximate volume of gel per calibration vessel for each method described. For a large number of calibration points, the large test tube (coaxial with beam) would be the preferable method, as numerous points can be obtained along its length. Otherwise, the short, thin test tube uses the least amount of gel, followed by the small vials and then the large test tube (perpendicular to beam), with the large flask method being the least efficient.

Setup varies in complexity for the differing methods. In this regard, the large flask method is the most preferable, being the least difficult to position for both irradiation and subsequent measurement. However, uncertainties associated with delivering known doses to small fields may be a significant issue. The other methods are all more complex as they necessarily require the use of a water phantom and a positioning structure. Such structures vary in the literature, but in general it is necessary to have something which locks the calibration vessels in position (particularly given their tendency to float) and interferes as little as possible with the beam. It is likely to be more cumbersome when the vessels must be positioned accurately at a specific depth within the water phantom. It is commonplace in the case of the small vials to irradiate multiple vessels in an array so as to reduce total beam-time, hence there is potential for the dose to be affected by the presence of neighbouring vials. Figures 2 and 3 indicate that centre-to-centre separation of vials of about 3 cm would result in a slightly increased dose to the gel. Centre-to-centre separation of 4 to 6 cm would be sufficient to reduce the possibility of scatter that influences the absorbed dose to a negligible level.

There are further considerations not explicitly investigated here. There has been recent work by Dumas *et al* (2006) that indicates that the use of smaller calibration vessels may result in a greater apparent dose than that exhibited by large phantoms for the same batch of gel, which they attribute to a higher local temperature generated from the exothermic polymerisation reaction. Furthermore, though the method employing a large test tube coaxial with the beam may seem preferable due to the large number of calibration points yielded, B1-field spatial inhomogeneities (Tincher *et al* 1993) in the MRI limit the length of the calibration tube that can be used without risking a loss of accuracy. Also, slice thickness when measuring calibration points should be as thin as possible such that less

accurate regions of gel are not included with accurate calibrations points; however, the compromise is that thin slices often lead to an increase in statistical noise.

5. Conclusion

This study has shown that the majority of gel calibration techniques examined, if performed under strict conditions, result in doses to gel that match equivalent doses in a water phantom to within one percent, with the exception of the method involving a long test tube coaxial with a beam, for which there exists a disparity ranging up to approximately two percent. Of the techniques examined, the preferable method, in terms of accuracy and ease of use, is likely to be that involving the use of a large diameter flask into which numerous small fields of varying dose are directed.

Acknowledgements

This work was supported by an Australian Research Council (ARC) Linkage Project (grant number LP0562315) and by the RMIT Foundation's Maxwell Eagle Fund.

References

Baldock C, Burford RP, Billingham N, Wagner GS, Patval S, Badawi RD and Keevil SF 1998 Experimental procedure for the manufacture and calibration of polyacrylamide gel (PAG) for magnetic resonance imaging (MRI) radiation dosimetry *Phys. Med. Biol.* **43** 695-702

Baldock C, Murry P and Kron T 1999 Uncertainty analysis in polymer gel dosimetry *Phys. Med. Biol.* **44** N243-N246

DeDeene Y, Hanselaer P, DeWagter C, Achten E and DeNeve W 2000 An investigation of the chemical stability of a monomer/polymer gel dosimeter *Phys. Med. Biol.* **45** 859-878

DeDeene Y, Reynaert N and DeWagter C 2001 On the accuracy of monomer/polymer gel dosimetry in the proximity of a high-dose rate 192Ir source *Phys. Med. Biol.* **46** 2801-2825

Dumas EM, Ghyslain L and Lepage M 2006 Effect of container size on the accuracy of polymer gel dosimetry *Proc. DOSGEL* (Quebec, Canada: 186-188 August 2006)

EGSnrc website (accessed February 2006), http://www.irs.inms.nrc.ca/EGSnrc/EGSnrc.html

Fong PM, Keil DC, Does MD and Gore JC 2001 Polymer gels for magnetic resonance imaging of radiation dose distributions at normal room atmosphere *Phys. Med. Biol.* **46** 3105-3113

Keall P and Baldock C 1999 A theoretical study of the radiological properties and water equivalence of Fricke and polymer gels used for radiation dosimetry *Australas. Phys. Eng. Sci. Med.* **22** 85-91

Low DA, Dempsey JF, Venkatesan R, Mutic S, Markman J, Haacke EM and Purdy JA 1999 Evaluation of polymer gels and MRI as a 3-D dosimeter for intensity-modulated radiation therapy *Med. Phys.* **26** 1542-1551

Love PA, Evans PM, Leach MO and Webb S 2003 Polymer gel measurement of dose homogeneity in the breast: comparing MLC intensity modulation with standard wedged delivery *Phys. Med. Biol.* **48** 1065-1074

Maryanski MJ, Schulz RJ, Ibbot GS, Gatenby JC, Xie J, Horton D and Gore JC 1994 Magnetic resonance imaging of radiation dose distributions using a polymer gel dosimeter *Phys. Med. Biol.* **39** 1437-1455

Maryanski MJ, Ibbott GS, Eastman P, Schulz RJ and Gore JC 1996 Radiation therapy dosimetry using magnetic resonance imaging of polymer gels *Med. Phys.* **25** 699-705

McJury M, Oldham M, Leach MO and Webb S 1999a Dynamics of polymerization in polyacrylamide gel (PAG) dosimeters: (I) ageing and long-term stability *Phys. Med. Biol.* **44** 1863-1873

McJury M, Tapper PD, Cosgrove VP, Murphy PS, Griffin S, Leach MO, Webb S and Oldham M 1999b Experimental 3D dosimetry around a high-dose rate clinical 192Ir source using a polyacrylamide gel (PAG) dosimeter *Phys. Med. Biol.* **44** 2431-2444

Metcalfe P, Kron T and Hoban P 1997 *The Physics of Radiotherapy X-Rays from Linear Accelerators* (Madison, WI: Medical Physics Publishing)

Michael GJ, Henderson CJ, Nitschke K and Baldock C 2000 Effects of glass and backscatter on measurement of absorbed dose in polyacrylamide gel (PAG) dosimeters *Phys. Med. Biol.* **45** N133-N138

Mohan R, Chen C and Lidofsky L 1985 Energy-angle distributions of accelerator photons *Med. Phys.* **12** 592-597

Nelson WR, Hirayama H, Rogers DWO, *The EGSnrc Code System: SLAC-265* (Stanford Linear Accelerator Center)

NIST website (accessed April 2006), http://physics.nist.gov/PhysRefData/XrayMassCoef/tab2.html

Oldham M, Baustert I, Lord C, Smith TAD, McJury M, Warrington AP, Leach MO and Webb S 1998a An investigation into the dosimetry of a nine-field tomotherapy irradiation using BANG-gel dosimetry *Phys. Med. Biol.* **43** 1113-1132

Oldham M, McJury M, Baustert IB, Webb S and Leach MO 1998b Improving calibration accuracy in gel dosimetry *Phys. Med. Biol.* **43** 2709-2720

Tincher M, Meyer CR, Gupta R and Williams DM 1993 Polynomial modelling and reduction of RF body coil spatial inhomogeneity in MRI *IEEE Trans. Med. Im.* **12** 361-366

Trapp JV, Bäck SÅJ, Lepage M, Michael G and Baldock C 2001 An experimental study of the dose response of polymer gel dosimeters imaged with x-ray computed tomography *Phys. Med. Biol.* **46** 2939-2951

Trapp JV, Michael G, DeDeene Y and Baldock C 2002 Attenuation of diagnostic energy photons by polymer gel dosimeters *Phys. Med. Biol.* **47** 4247-4258

Trapp JV, Partridge M, Hansen VN, Childs P, Bedford J, Warrington AP, Leach MO and Webb S 2004c The use of gel dosimetry of electron and photon treatment plans in carcinoma of the scalp *Phys. Med. Biol.* **49** 1625-1635

Trapp JV, Michael G, Evans PM, Baldock C, Leach MO and Webb S 2004a Dose resolution in gel dosimetry: effect of uncertainty in the calibration function *Phys. Med. Biol.* **49** N139-N146

Trapp JV, Warrington AP, Partridge M, Philps A, Glees J, Tait D, Ahmed R, Leach MO and Webb S 2004b Measurement of the three-dimensional distribution of radiation dose in grid therapy *Phys. Med. Biol.* **49** N317-N323

Vergote K, DeDeene Y, Duthoy W, DeGersem W, DeNeve W, Achten E and DeWagter C 2004 Validation and application of polymer gel dosimetry for the dose verification of an intensity-modulated arc therapy (IMAT) treatment *Phys. Med. Biol.* **49** 287-305

Captions

Table 1 Density and elemental composition of materials modelled.

Table 2 The dose to gel is consistently lower than that to water. Dose is averaged over an area of 80 mm^2 about the central axis with a voxel thickness of 3 mm (away from the walls of the test tube). The percentage difference between the dose delivered to the gel and that delivered to an equivalent volume of water as it varies along the length of the test tube is given in the table below.

Table 3 Details of the gel models, including geometrical arrangement, calibration vessel dimensions, optimal post-irradiation measurement method and degree of disparity between the dose to gel and dose to an equivalent volume of water.

Figure 1 Diagrams showing the details of the model geometries (not to scale). 1(a) shows the arrangement for a small vial of PAG at the surface of a water phantom (Method A). 1(b) shows the same vial at a depth of 5 cm below the water surface (Method B). 1(c) shows a large test tube irradiated down its axis such that a depth dose curve is achieved along its length (Method C). 1(d) is a large test tube at the surface of a water phantom, irradiated along its axis (Method D). 1(e) is a similar arrangement, with a test tube of smaller diameter and length (Method E). In all cases, the polyethylene lid is 11 mm long. 1(f) is a large Perspex tub (shown with Nitrogen gap) irradiated though the base with a small field (Method F).

Figure 2 Small vial of PAG at the surface of a water phantom, irradiated through base. Fig. 2(a)(i) shows the depth dose curve through this arrangement (in black, bold) and the depth dose curve through water alone, while Fig. 2(a)(ii) is the ratio of the former curve to the latter. There is a statistical uncertainty at D_{max} is 0.07 % for the dose distribution and 0.15 % (maximum) for the ratio. Fig. 2(b)(i) displays the dose radially outward from the central axis of the vial, with the equivalent curve through water, taken at a slice through the mid-point of the vial and 2(b)(ii) is the corresponding ratio to dose in water.

Figure 3 Small vial of PAG at 5 cm depth in a water phantom, irradiated through base. Fig. 3(a)(i) shows the depth dose curve through this arrangement (in black, bold) and the depth dose curve through water alone, while Fig. 3(a)(ii) is the ratio of the former curve to the latter. There is a statistical uncertainty of 0.25 % at D_{max}. Fig. 3(b)(i) displays the dose radially outward from the central axis of the vial, with the equivalent curve through water, taken at a slice through the mid-point of the vial. 3(b)(ii) is the corresponding ratio of the vial system dose distribution to the water dose distribution.

Figure 4 Long test tube of PAG with its base at the surface of a water phantom, irradiated along its axis. Fig. 4(a)(i) shows the depth dose curve through this arrangement (in black, bold) and the depth dose curve through water alone, while Fig. 4(a)(ii) is the ratio of the former curve to the latter. There is a statistical uncertainty of 0.23 % at D_{max}. Fig. 4(b)(i, iii and v) display the dose radially outward at respective depths of 5, 10 and 15 cm down the test tube, with the equivalent dose in water alone, and 4(b)(ii, iv and vi) are the corresponding ratios of the former to the latter curves.

Figure 5 Test tubes of PAG at a depth of 5 cm in a water phantom, irradiated perpendicular to test tube axis. Fig. 5(a)(i) shows the depth dose curve along the axis of a test tube of diameter 2.5 cm and length 20 cm (in black, bold) and the dose distribution through water alone. Fig. 5(a)(ii) is the ratio of the former curve to the latter. Fig. 5(b)(i) shows the dose distribution along the axis of a test tube of diameter 1.0 cm and length 10 cm (in black) and the dose distribution through water alone. Fig. 5(b)(ii) is the ratio of the two curves.

Figure 6 Large flask of PAG in air, irradiated with a 2 cm field along the central axis of the flask. Fig. 6(a)(i) shows the depth dose curve along the axis of the flask (in black, bold) and the depth dose curve through water alone. Fig. 6(a)(ii) is the ratio of the former curve to the latter. Fig. 6(b)(i) shows the radial dose distribution out from the central axis (in black) and the depth dose curve through water alone (in blue), taken at a line through D_{max}. Fig. 6(b)(ii) is the ratio of the two curves.

Table 1

Material	Density ($g.cm^{-3}$)	Elemental composition (% mass)									
		H	B	C	N	O	Na	Ar	Al	Si	K
Air	1.204×10^{-3}			0.0124	75.52	23.18		1.28			
Nitrogen	1.1653×10^{-3}				100.00						
PAG	1.02	10.70		4.70	1.70	82.90					
Perspex	1.19	8.05		59.98		31.96					
Polyethylene	0.93	14.37		85.63							
Pyrex	2.23		4.01			53.96	2.82		1.16	37.72	0.33
Water	1.00	11.10				88.90					

Table 2

Large test tube (coaxial with beam)	
Depth in test tube (cm)	**Difference between measured dose and dose to water**
5	0.7 ± 0.2 %
10	1.1 ± 0.3 %
15	2.0 ± 0.3 %

Table 3

	Calibration model					
	Small vial (at water surface)	Small vial (5cm deep in water)	Large test tube (coaxial with beam)	Large test tube (perpendicular to beam)	Thin test tube (perpendicular to beam)	Large flask (coaxial with beam)
Construction	Pyrex vial with polyethylene lid		Pyrex culture tube with polyethylene lid		Pyrex culture tube with polyethylene lid	Perspex flask
Dimensions	Internal diameter: 25 mm Wall thickness: 1.0 mm Length: 55 mm		Internal diameter: 25 mm Wall thickness: 1.0 mm Length: 200 mm		Internal diameter: 10 mm Wall thickness: 1.0 mm Length: 100 mm	Internal diameter: 130 mm Wall thickness: 6.0 mm Length: 57 mm
Approximate volume of gel (cm^3) per vessel	30		100		10	3030
Geometrical arrangements (including beam radius modelled)	At surface of water phantom, irradiate through base (Beam radius: 50 mm)	5 cm deep in water phantom, irradiate through base (Beam radius: 50 mm)	At surface of water phantom, irradiate through base coaxial with beam (Beam radius: 50 mm)	5 cm deep in water phantom, irradiate with axis perpendicular to that of beam (Beam radius: 150 mm)	5 cm deep in water phantom, irradiate with axis perpendicular to that of beam (Beam radius: 100 mm)	Align coaxial with beam and irradiate with small beamspot (Beam radius: 10 mm)
Dose measurement method: area of voxels and location	Average 80 mm^2 area at D_{max}	Average 80 mm^2 area mid-vial	Average 80 mm^2 area at varying depths	Average 13 mm^2 area (about central axis) along length of test tube	Average 13 mm^2 area (about central axis) along length of test tube	Average 80 mm^2 area at D_{max}
Difference between calculated dose to gel and dose to water	0.7 (± 0.2) %	0.4 (± 0.2) %	Varies with depth in test tube (see Table 2)	0.7 (± 0.1) %	0.4 (± 0.3) %	0.2 (± 0.1) %

Figure 1

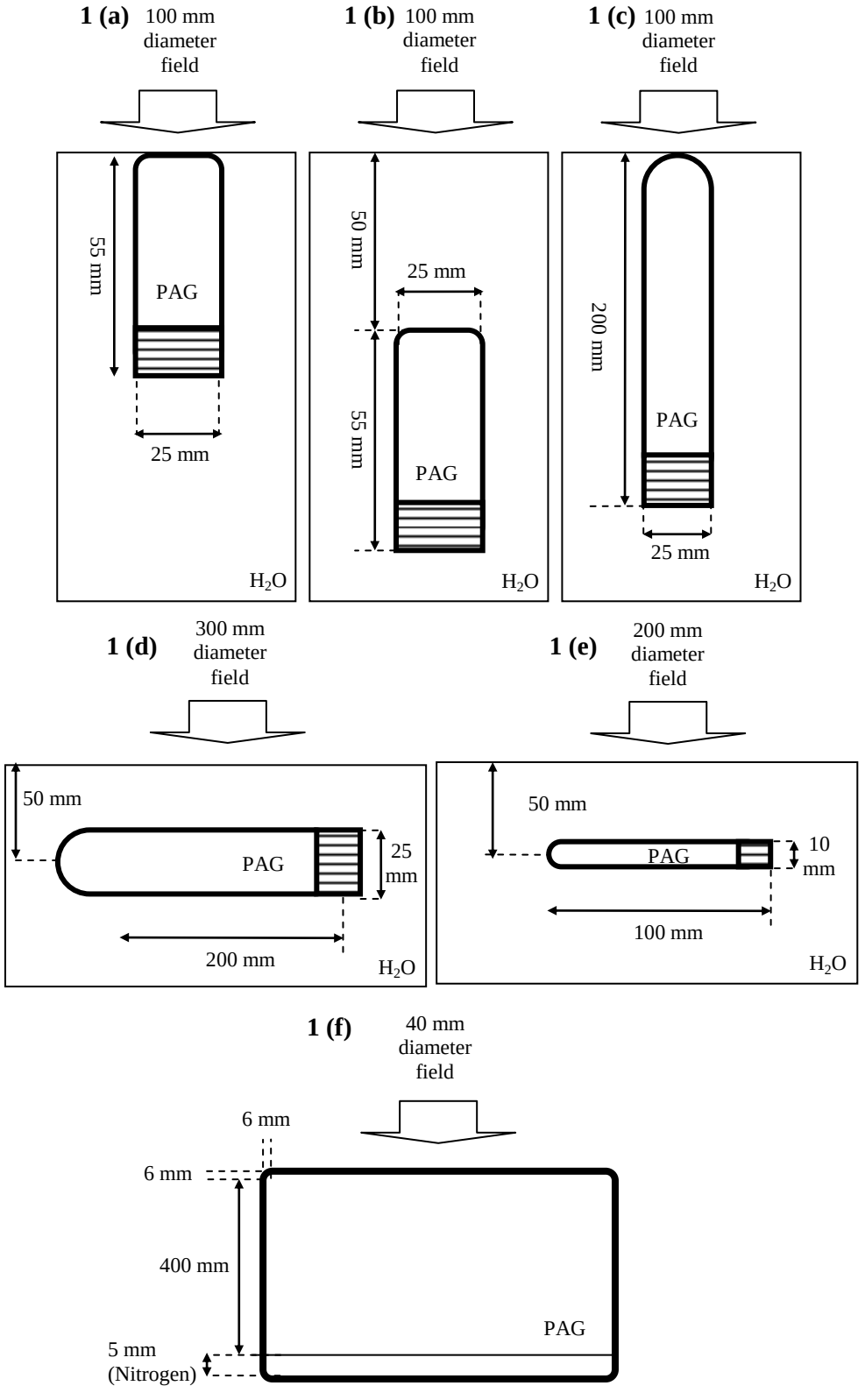
1 (a)
100 mm diameter field
55 mm
PAG
25 mm
H2O
1 (b)
100 mm diameter field
50 mm
25 mm
55 mm
PAG
H2O
1 (c)
100 mm diameter field
200 mm
PAG
25 mm
H2O
1 (d)
300 mm diameter field
50 mm
PAG
25 mm
200 mm
H2O
1 (e)
200 mm diameter field
50 mm
PAG
10 mm
100 mm
H2O
1 (f)
40 mm diameter field
6 mm
6 mm
400 mm
PAG
5 mm
(Nitrogen)

Figure 2

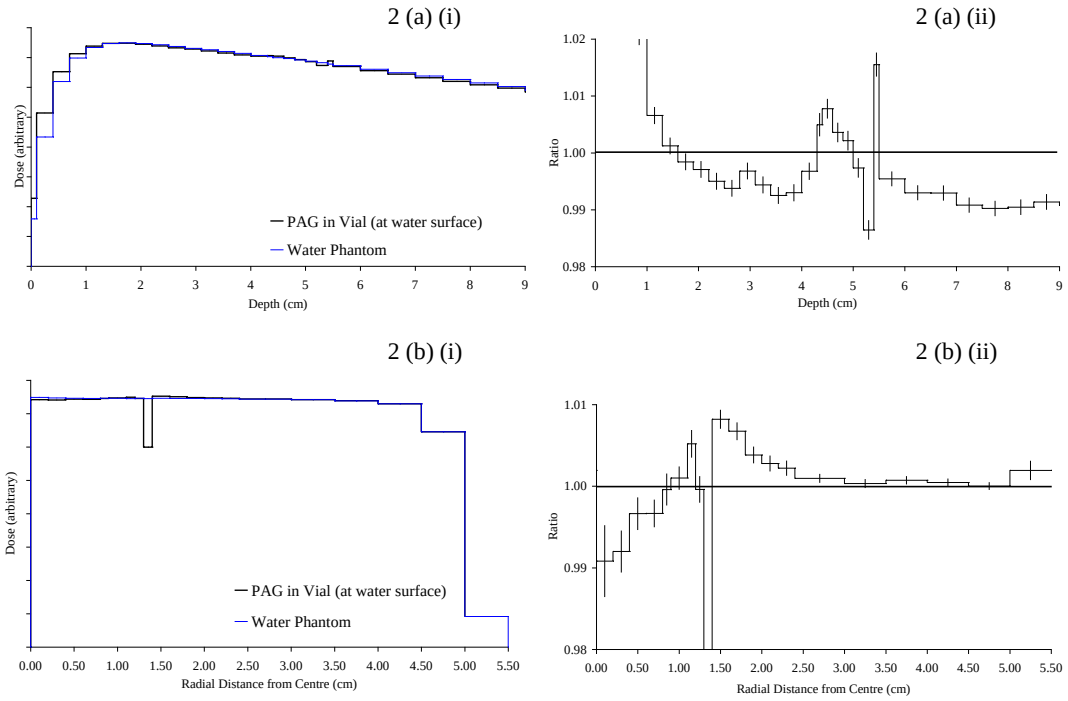
2 (a) (i)
Dose (arbitrary)
PAG in Vial (at water surface)
Water Phantom
Depth (cm)
2 (a) (ii)
Ratio
Depth (cm)
2 (b) (i)
Dose (arbitrary)
PAG in Vial (at water surface)
Water Phantom
Radial Distance from Centre (cm)
2 (b) (ii)
Ratio
Radial Distance from Centre (cm)

Figure 3

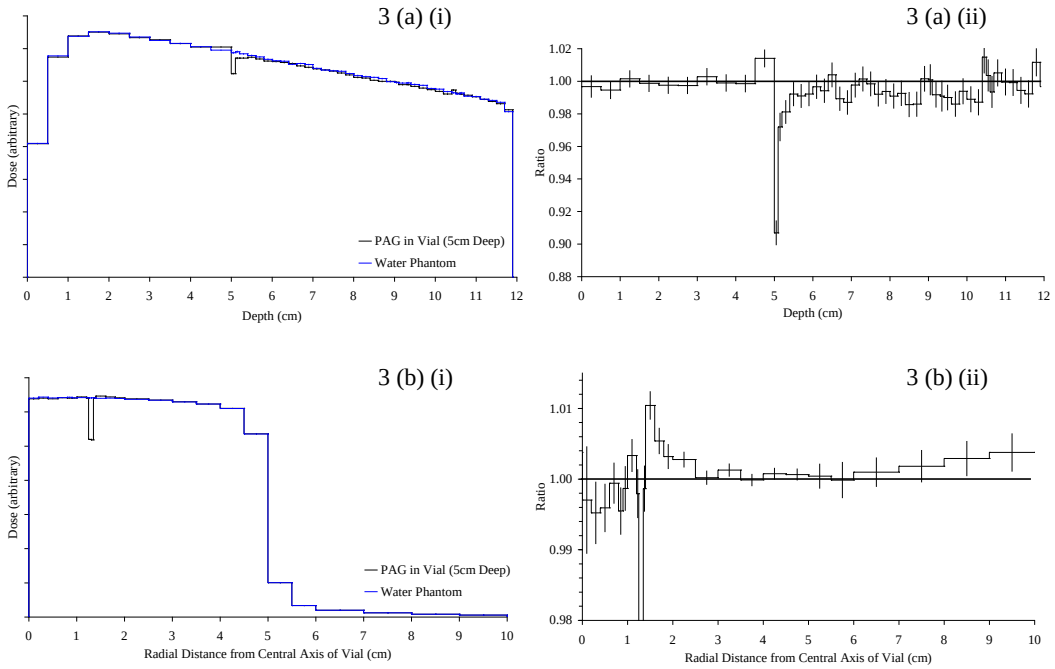
3 (a) (i)
Dose (arbitrary)
PAG in Vial (5cm Deep)
Water Phantom
Depth (cm)
3 (a) (ii)
Ratio
Depth (cm)
3 (b) (i)
Dose (arbitrary)
PAG in Vial (5cm Deep)
Water Phantom
Radial Distance from Central Axis of Vial (cm)
3 (b) (ii)
Ratio
Radial Distance from Central Axis of Vial (cm)

Figure 4

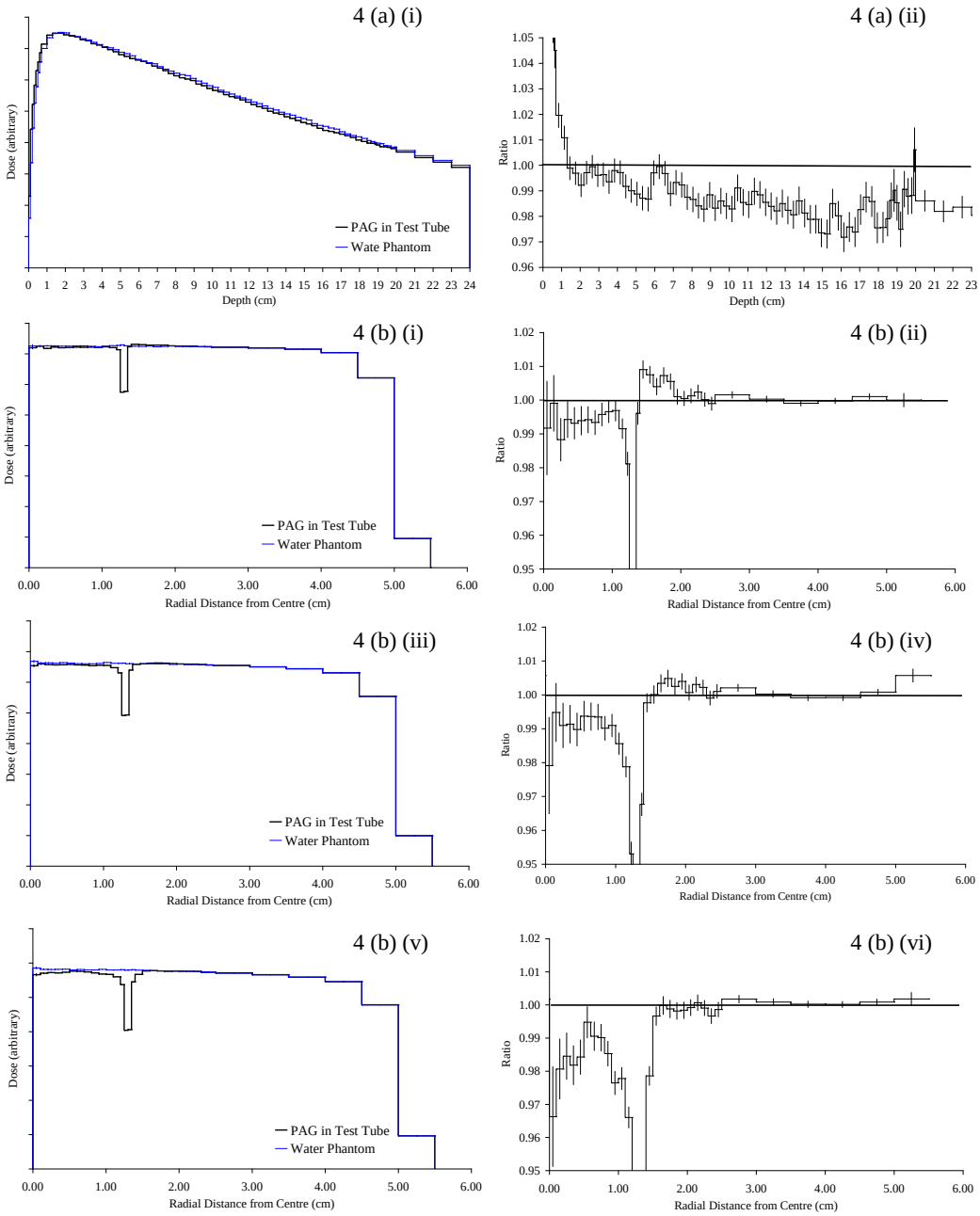
4 (a) (i)
Dose (arbitrary)
PAG in Test Tube
Wate Phantom
Depth (cm)
4 (a) (ii)
Ratio
Depth (cm)
4 (b) (i)
Dose (arbitrary)
PAG in Test Tube
Water Phantom
Radial Distance from Centre (cm)
4 (b) (ii)
Ratio
Radial Distance from Centre (cm)
4 (b) (iii)
Dose (arbitrary)
PAG in Test Tube
Water Phantom
Radial Distance from Centre (cm)
4 (b) (iv)
Ratio
Radial Distance from Centre (cm)
4 (b) (v)
Dose (arbitrary)
PAG in Test Tube
Water Phantom
Radial Distance from Centre (cm)
4 (b) (vi)
Ratio
Radial Distance from Centre (cm)

Figure 5

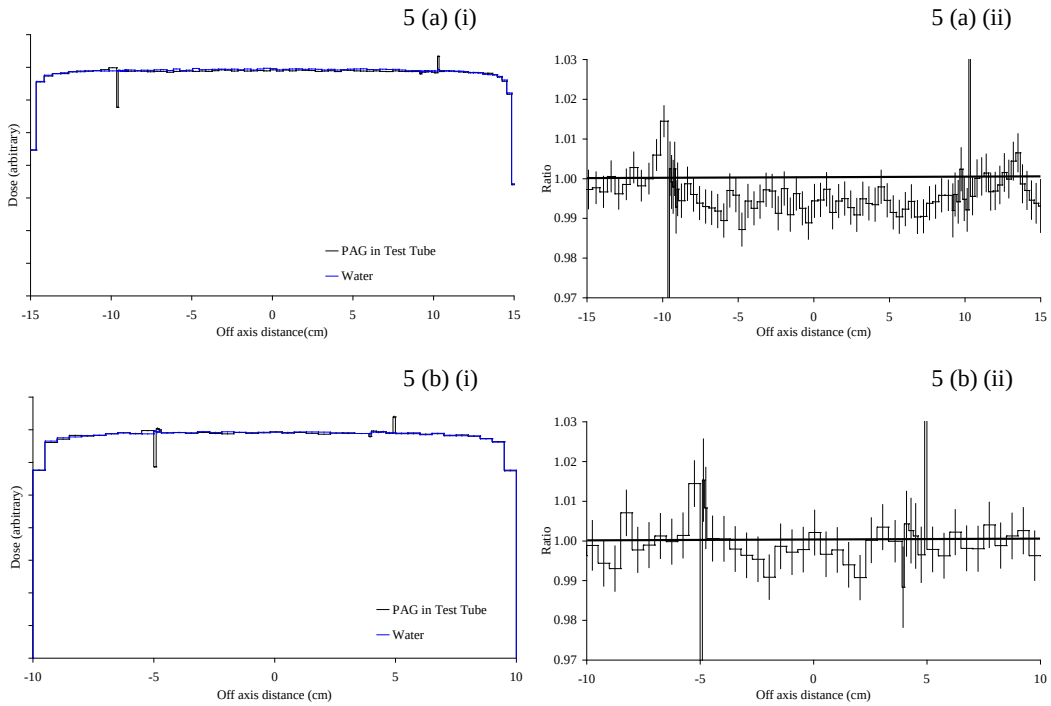
5 (a) (i)
5 (a) (ii)
Dose (arbitrary)
PAG in Test Tube
Water
Off axis distance(cm)
Ratio
Off axis distance (cm)
5 (b) (i)
5 (b) (ii)
Dose (arbitrary)
PAG in Test Tube
Water
Off axis distance (cm)
Ratio
Off axis distance (cm)

Figure 6

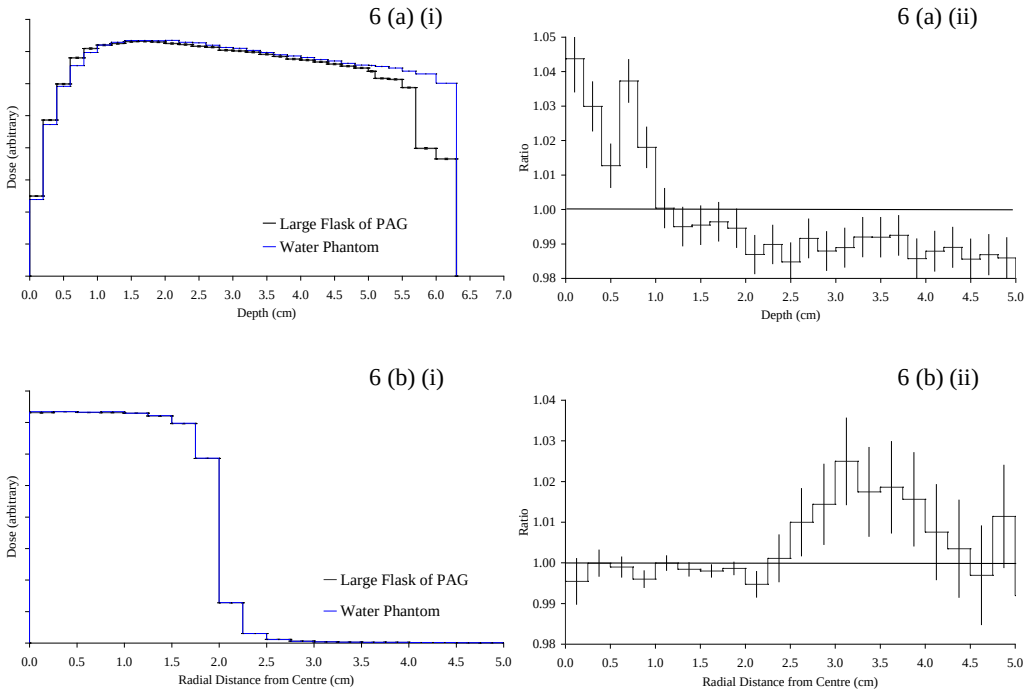
6 (a) (i)
Dose (arbitrary)
Large Flask of PAG
Water Phantom
Depth (cm)
6 (a) (ii)
Ratio
Depth (cm)
6 (b) (i)
Dose (arbitrary)
Large Flask of PAG
Water Phantom
Radial Distance from Centre (cm)
6 (b) (ii)
Ratio
Radial Distance from Centre (cm)